Journal of Materials Chemistry

Cite this: J. Mater. Chem., 2011, 21, 11142

www.rsc.org/materials

PAPER

Superparamagnetic magnetite nanocrystal clusters as potential magnetic carriers for the delivery of platinum anticancer drugs

Ruimin Xing,[ab] Xiaoyong Wang,*[c] Changli Zhang,[ad] Jinzhuan Wang,[a] Yangmiao Zhang,[a] You Song[a] and Zijian Guo*[a]

Received 1st April 2011, Accepted 11th May 2011
DOI: 10.1039/c1jm11369k

Magnetic nanoparticles are promising carriers for targeted drug delivery. Superparamagnetic magnetite nanocrystal clusters modified with sodium carboxymethylcellulose were prepared by an *in situ* hydrothermal procedure in this study. The composition, morphology, and magnetic property of the clusters have been characterized by SEM, TEM, XRD, XPS, TGA, IR, and SQUID. The clusters display excellent dimensional uniformity, strong magnetisability, good aqueous dispersibility, and modifiable functionality. By virtue of the abundant carboxylate groups on the surface of the clusters, dechlorinated cisplatin was tethered to the superparamagnetic nanoparticles. The formation and the magnetism of the conjugate have been confirmed by zeta potential, EDX, ICP-MS, XPS, and SQUID. The magnetic property is well retained in the drug-loaded clusters. In comparison with cisplatin, the conjugate can more readily enter cancer cells and exert higher cytotoxicity towards the human cervical cancer HeLa cells and the human hepatocarcinoma HepG2 cells. These nanoparticles are likely to be used as targeted carriers to deliver platinum anticancer drugs.

Introduction

Cisplatin [*cis*-dichlorodiammineplatinum(II), CDDP] has played a crucial role in the chemotherapy of various malignant tumors since its discovery over 40 years ago.[1] However, the therapeutic window of CDDP is exceedingly narrowed by severe systemic toxicity owing to its indiscriminate body distribution in the treatment.[2] Tremendous attempts have been made to improve the selectivity of platinum drugs for tumors by integrating target functionality into the drug structures or developing targeted drug delivery systems.[3,4] Among them, magnetic drug delivery systems have evoked intensive interest in recent years because they are supposed to guide drugs preferentially to their biological target through external magnets and hence abate the lesions in normal tissues.[5] The fabrication of proper magnetic nanoparticles is the foremost step to achieve this goal.

Superparamagnetic iron oxide nanoparticles (SPION) have proved to be promising magnetic drug carriers in virtue of their biocompatibility, biodegradability, aqueous dispersibility and magnetisability.[6] After coating with biocompatible materials, SPION could coordinate with therapeutic or diagnostic moieties to form targeted formulations.[7] Nevertheless, the synthesis of these formulations is often complicated and difficult.[6c] For example, additional surface modifications are usually needed to transform the hydrophobic nanoparticles into hydrophilic ones for biomedical applications.[6e] Moreover, most monodisperse SPION prepared as drug carriers are synthesized at high temperature in organic solvents with a diameter of around 10 nm,[6a] which implies that individual nanoparticles prepared by these methods only possess a small magnetic moment and could not be effectively separated from the solution. More unfavorably, on account of the low magnetization, it is difficult to manipulate the movement of nanoparticles in the blood by a moderate magnetic field, which limits their practical use as targeted drug carriers.[8]

Recently, the development of innovative magnetic cores and improvement of particulate morphology have become the major avenues to enhance the magnetization of nanoparticles.[9] For instance, when SPION assembled together to form clusters, their magnetic moment would rise.[9c] However, a dilemma appears in SPION: to increase the magnetization but not to induce the superparamagnetic–ferromagnetic transition, so that they could maintain dispersibility in solution.

In this work, superparamagnetic magnetite nanocrystal clusters modified with sodium carboxymethylcellulose (CMC-SPMNCs) are fabricated as nanocarriers for the delivery of

[a]*State Key Laboratory of Coordination Chemistry, School of Chemistry and Chemical Engineering, Nanjing University, Nanjing, 210093, PR China. E-mail: zguo@nju.edu.cn; Fax: +86 25 83314502; Tel: +86 25 83594549*
[b]*Institute of Molecular and Crystal Engineering, College of Chemistry and Chemical Engineering, Henan University, Kaifeng, 475001, PR China*
[c]*State Key Laboratory of Pharmaceutical Biotechnology, School of Life Sciences, Nanjing University; State Key Laboratory of Analytical Chemistry for Life Science, Nanjing University, Nanjing, 210093, PR China. E-mail: boxwxy@nju.edu.cn; Fax: +86 25 83224539*
[d]*Nanjing Xiaozhuang College, Nanjing, 210071, PR China*

platinum drugs. Nanocrystal clusters have the merit of increasing the magnetization in a controllable manner while retaining the superparamagnetic characters of magnetite. Sodium carboxymethylcellulose (CMC-Na) was selected because it is a biocompatible and biodegradable polymer with abundant carboxylate groups that can coordinate with iron ions or link up platinum moieties. The platinum pharmacophore, *viz*. dechlorinated CDDP [*cis*-monochlorodiammineplatinum(II), CMDP], was loaded onto the clusters by reacting it with the carboxylate groups on the surface of the particles, forming a magnetic conjugate CMDP–CMC–SPMNC (Scheme 1). The conjugate exhibits an enhanced cytostatic effect against tumor cells as compared with cisplatin.

Experimental section

Materials

CDDP was obtained from Shandong Boyuan Chemical Co., Ltd. $FeCl_3 \cdot 6H_2O$, anhydrous sodium acetate (NaAc), ethylene glycol (EG), sodium carboxymethylcellulose (CMC-Na) and other chemical reagents were of analytical grade and used as received without further purification. Doubly deionized water (18.2 MΩ*cm at 25 °C) prepared on a Milli-Q (MQ) water system was used throughout all experiments.

Preparation and characterization of CMC-SPMNCs

CMC-SPMNCs were prepared *via* a one-pot hydrothermal method. In a typical procedure, $FeCl_3 \cdot 6H_2O$ (0.68 g), CMC-Na (0.5 g) and anhydrous NaAc (1.6 g) were orderly dissolved in EG (20 mL). The mixture was stirred vigorously in an ultrasonicator to give a clear brown yellow solution, which was transferred into a Teflon-lined autoclave, sealed, kept at 200 °C for 12 h, and cooled to room temperature. The solid black product was collected by magnetic separation, washed, at least three times, with water and ethanol and dried under vacuum at room temperature.

The scanning electron microscopy (SEM) images were taken using an Hitachi S-4800 field emission electron microscope at an accelerating voltage of 5 kV. The transmission electron microscopy (TEM) images and patterns of selected area electron diffraction (SAED) were obtained using a JEOL JEM-2100 transmission electron microscope at an accelerating voltage of 200 kV. Samples for TEM and SAED were prepared by dripping a droplet of dilute sample alcohol solution (5 μL) onto a carbon-coated copper grid and drying at room temperature. The X-ray powder diffraction (XRD) patterns were recorded on a Japan Shimadzu XRD-6000 diffractometer in the 2θ range of 20–70° with Cu Kα radiation ($\lambda = 0.15418$ nm) and a scanning rate of 0.05 deg s^{-1}. X-Ray photoelectron spectra (XPS) were acquired on a Thermo ESCALAB 250 electron spectrometer with 150 W monochromatized Al Kα radiation (1486.6 eV), where all peaks were referred to the signature C1s peak for adventitious carbon at 284.8 eV. Thermal gravimetric analysis (TGA) was measured on a Pyris 1 TGA instrument with a heating rate of 20 °C min^{-1} in a nitrogen flow (20 mL min^{-1}). Derivative thermogravimetry (DTG) was deduced from the first derivative of the thermogravimetric (TGA) curve. FT-IR spectra were recorded on a Nicolet 6700 Fourier transform infrared spectrograph in the range of 4000–500 cm^{-1}. Magnetic measurements were carried out on the superconducting quantum interference device (SQUID, Quantum Design) magnetometer at 300 K.

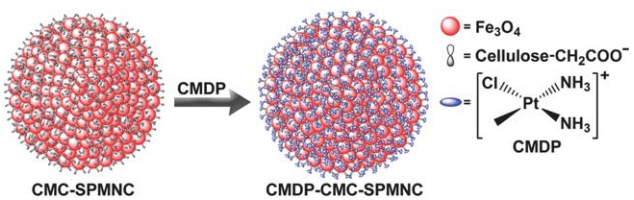

Scheme 1 Fabrication route of the CMDP–CMC–SPMNC conjugate.

Preparation and characterization of CMDP–CMC–SPMNCs

CDDP (30 mg) and $AgNO_3$ (15 mg) were dissolved in water (3 mL) and stirred in the dark at room temperature overnight. The resultant suspension was centrifuged to remove the precipitate and the dechlorinated cisplatin (CMDP) was acquired in the supernatant. CMC–SPMNCs were dispersed in the solution of CMDP and sonicated to give a suspension, which was stirred at 200 rpm for *ca* 100 h after the pH was adjusted to near neutral with NaOH (2 M). The obtained CMDP–CMC–SPMNCs were purified with a magnet and washed with water for at least five times under sonication to remove the redundant CMDP. Exhaustive separation was ensured by detecting platinum content in the supernatant with the inductively coupled plasma mass spectrometry (ICP-MS). Hydrodynamic diameters were determined using a BI-200SM dynamic light scattering (DLS, Brookhaven Instruments Co., Holtsville, NY).

SEM, XPS, and magnetic properties were determined as described for CMC-SPMNCs. Energy dispersive X-ray spectrum (EDX) was recorded on Hitachi S-4800 field emission electron microscope at an accelerating voltage of 20 kV. The zeta potential (ζ) was measured in water using a Malven Nano-Z instrument. The loading ratio of Pt to Fe was determined by ICP-MS using a standard Plasma-Quad II instrument (VG Elemental, Thermo Optek Corp.). The nitrolysis of the samples was carried out with a mixture of concentrated HNO_3 and HCl (1 : 3, v/v) at 95 °C for 2 h. The average of three replicates was taken as the final result.

Cytotoxicity assay

The cytotoxicity of CMDP–CMC–SPMNCs was tested by the 3-(4,5-dimethylthiazol-2-yl)-2,5-diphenyltetrazolium bromide (MTT) assay with CDDP and CMC–SPMNCs as the references. Briefly, the human cervical cancer cell line HeLa and the human hepatocarcinoma cell line HepG2 were seeded respectively in 96-well plates at 5000 cells per well in Dulbecco's modified Eagle's medium and incubated at 37 °C in the humidified atmosphere with 5% CO_2 for 12 h. The cells were then treated in triplicate with fresh medium containing grade concentrations of CMDP–CMC–SPMNCs, CDDP (in terms of Pt) and CMC–SPMNCs, respectively. Aliquot of MTT (10 μL, 5 mg mL^{-1}) in the phosphate buffered saline (PBS) were added to each of the wells after the cells were incubated at 37 °C for 72 h. The supernatant was taken off after 4 h of incubation and DMSO (150 μL) was added

to each well. The amount of the resultant MTT formazan was determined at 490 nm using an ELISA plate reader. The cytotoxicity was calculated based on the data of three replicate tests.

Cellular uptake

HeLa cells were seeded into a 12-well plate at 10^5 cells per well and incubated overnight. The medium was refreshed (1 mL per well) and the cells were treated with CMDP–CMC–SPMNCs and CDDP, respectively, at the IC_{50} concentration of the former (0.9 μM) and incubated at 37 °C for 6, 12, and 24 h, respectively. The medium was removed and the cells were incubated with trypsin solution for 1 min. After digestion, the cells were rinsed with PBS (1 mL × 3) and counted using trypan blue staining. The harvested cells were dispersed in water (50 μL) and nitrolyzed by adding HNO_3 (70 μL, 16 M) into the solution and heating at 95 °C for 2 h. The solution was then treated with H_2O_2 (20 μL, 30%) at 95 °C for 2 h and with HCl (35 μL, 12 M) at 37 °C for 0.5 h. The content of Fe and Pt was determined by ICP-MS after dilution to 1.00 mL. The average of three independent results was taken as the final value for Fe and Pt.

Prussian blue staining

HepG2 cells were seeded into a 6-well plate at 10^4 cells per well and incubated overnight. The medium was refreshed (1.5 mL per well) and the cells were treated with CMDP–CMC–SPMNCs at the IC_{50} concentration and incubated at 37 °C for 72 h. Prussian blue staining was performed by Prussian blue iron stain kit (Polysciences) according to the manufacturer's instruction. The image of the stained cells was captured by Olympus DP70 inverted microscope equipped with an Uplan FLN 40X0.75 objective (Olympus).

Results and disscussion

Preparation and characterization of CMC–SPMNCs

The preparation of CMC–SPMNCs is quite simple, in that the reactants $FeCl_3 \cdot 6H_2O$ and CMC-Na only need to react in the autoclave in the presence of NaAc and a polar solvent EG. NaAc acts as the alkali source to facilitate the hydrolysis of $FeCl_3$, and EG provides the reductive ambiance at high temperature. Under these conditions, the hydrolytic product $Fe(OH)_3$ is partially reduced to $Fe(OH)_2$, and further transforms into Fe_3O_4 after dehydration. At the same time, some unhydrolyzed $FeCl_3$ and unreduced $Fe(OH)_3$ undergo metal displacement reactions with CMC-Na, forming CMC-Fe complexes.[10] Fe_3O_4 and CMC-Fe spontaneously aggregate to form the crystalline "magnetite–CMC-Fe" nanocomposite. These primary nanocrystals nucleate in the supersaturated solution and finally aggregate into larger secondary particles, *i.e.* nanocrystal clusters.[9c] In contrast to other methodologies,[6b,6d] CMC–SPMNCs in this work were prepared by a one-pot method, which greatly simplifies the synthetic procedures for magnetic nanoparticles.

The morphology and size distribution of CMC–SPMNCs were investigated using SEM. As Fig. 1A presents, CMC–SPMNCs show an excellent monodispersity and a well-defined uniform spherical shape on a large scale. Statistical analyses indicate that the particles have a relatively narrow distribution, with an average diameter of about 180 nm (inset in Fig. 1A). The high-resolution SEM image in Fig. 1B demonstrates that the nanospheres consist of many primary nanoparticles in the order of 8–10 nm and therefore have the structural character of clusters.

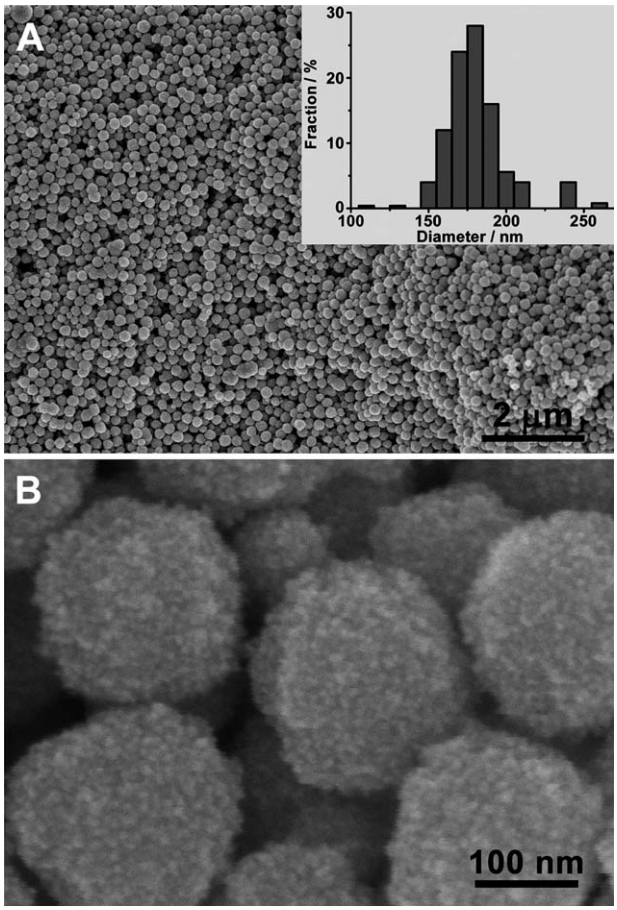

Fig. 1 Low- (A) and high-resolution (B) SEM images of CMC–SPMNCs. Inset in A shows the size distribution of CMC–SPMNCs on the basis of statistical analyses.

The structure of the clusters was further confirmed by TEM. As the representative TEM image shown in Fig. 2A, the "magnetite–CMC-Fe" nanocrystals aggregate to form a spherical three-dimensional cluster. The SAED pattern (inset in Fig. 2A) obtained from an isolated nanosphere indicates that the cluster adopts a cubic structure with polycrystaline-like diffraction profiles. A close inspection of the nanosphere by the high-resolution TEM confirms that the monodisperse clusters are composed of small primary particles (Fig. 2B). These particles display high crystallinity and assemble randomly to form the cluster. Clear crystal lattice fringes with the spacings of 0.251 and 0.296 nm are observed, which are consistent with the values for (311) and (220) planes of a cubic magnetite phase, respectively.

The crystal structure of the clusters was also studied by XRD and XPS analyses.[11] In the XRD spectrum (Fig. 3A), all diffraction peaks and positions match well with those from the JCPDF card (No. 01-1111) for the cubic-phase magnetite. Calculations using the Debye–Scherrer formula for the strongest peak (311) give a grain size of 8 nm, which is comparable to the SEM statistical value. This result fully supports the SEM and

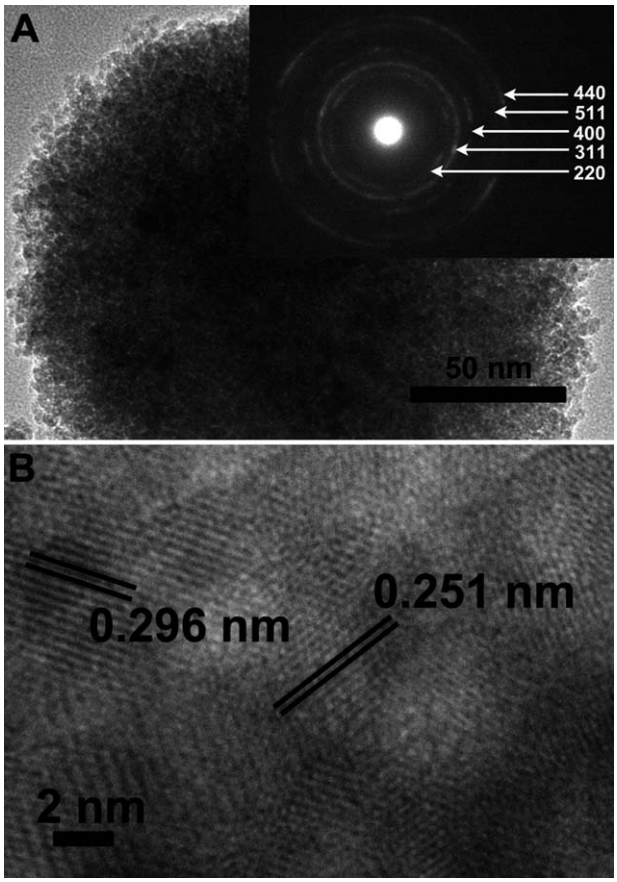

Fig. 2 Typical (A) and high-resolution TEM (B) images of CMC–SPMNCs. Inset in A is the SAED pattern of an isolated cluster.

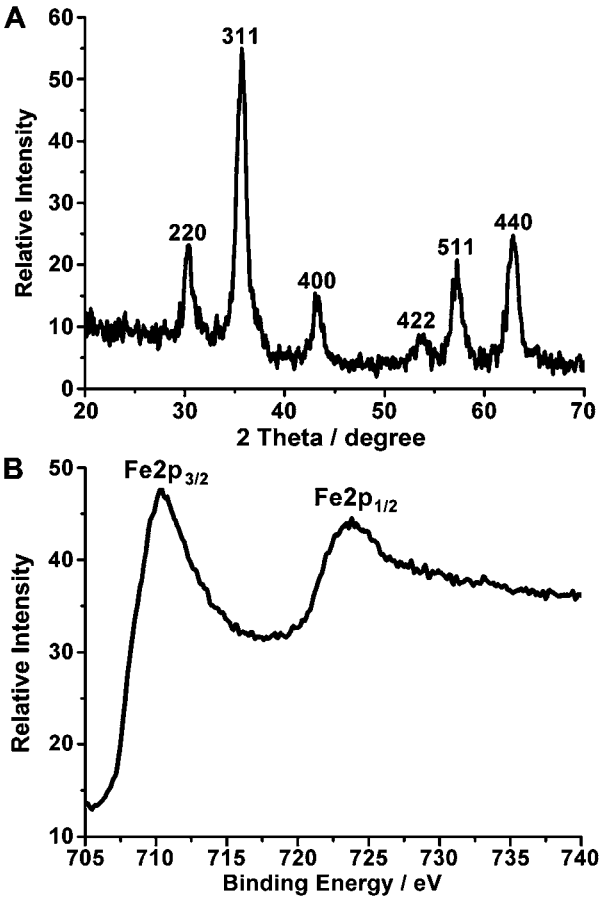

Fig. 3 The XRD pattern (A) and XPS spectrum of Fe2p (B) for CMC–SPMNCs.

TEM observations that the clusters are made up of primary particles. XPS spectroscopy was used to determine the crystal phase and composition of the clusters in order to verify the product is magnetite (Fe_3O_4) rather than maghemite (γ-Fe_2O_3), because they both show magnetic behavior and have similar XRD patterns.[11a] As shown in Fig. 3B, the binding energy values of $Fe2p_{3/2}$ and $Fe2p_{1/2}$ photoelectron peaks are 710.3 and 723.8 eV, respectively, which are close to the reported values for Fe_3O_4. Particularly, the absence of a charge transfer satellite near the photoelectron peak of $Fe2p_{3/2}$ manifests that iron is at a mixed oxidation state in the clusters.[11c]

The thermal stability of CMC–SPMNCs was investigated by TGA and DTG to examine whether CMC is involved in the clusters. The thermograms of CMC–SPMNCs and CMC-Na are shown in Fig. 4. CMC–SPMNCs exhibit a remarkably broad decomposition temperature as compared with that of CMC–Na, which shows a very steep curve around 300 °C. In the test temperature range (0–800 °C), CMC–SPMNCs only lose *ca* 20% weight; whereas CMC-Na loses 50% weight at ~310 °C and *ca* 70% weight at 800 °C. The broad decomposition temperature of CMC–SPMNCs may be attributed to the coordination of carboxylate groups of CMC with iron, and also to the embedment of CMC-Fe complexes in the nanospheres. DTG is useful for observing slight changes in weight that are not readily noticed on the TGA thermograms. In DTG, the rate of percent weight loss *versus* time (dw/dt) is obtained from the first derivative of the TGA curve.[12] As the dashed lines in Fig. 4 show, CMC–SPMNCs displays a relatively flat DTG plot as a whole. Two small peaks appear at 300 and 670 °C, respectively, which suggests that CMC on the surface of the clusters decomposes at 300 °C, while that buried within the clusters decomposes at 670 °C. CMC-Na presents a large, sharp peak at 300 °C on the

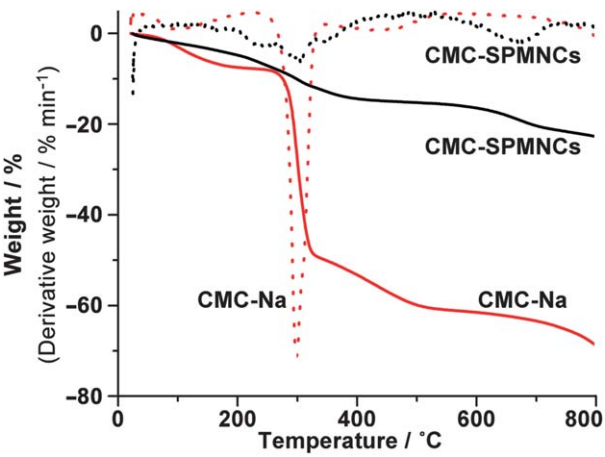

Fig. 4 The TGA thermograms (solid line) and the corresponding DTG plots (dashed line) of CMC–SPMNCs and CMC-Na.

DTG plot. The peak protrudes rapidly and then returns abruptly to the zero baseline. At the inflection point on the DTG curve, the weight of CMC-Na loses most rapidly. The consistency of the inflection point at 300 °C on the DTG plot of CMC–SPMNCs and CMC-Na suggests that the clusters contain the CMC component with weight percent accounting for *ca* 20% of the clusters.

The involvement and coordination of CMC in the nanoclusters were further studied by IR spectroscopy. As seen in Fig. 5, in comparison with the IR spectrum of CMC-Na, CMC–SPMNCs shows the typical absorptions of the cellulose backbone and carboxyl methyl ether group at 1611 cm^{-1}. The broad absorption band at 3400 cm^{-1} is attributed to the stretching frequency of the –OH group as well as intra- and intermolecular hydrogen bonds. The bands at 2907 cm^{-1} are due to the C–H stretching vibration; those around 1411 and 1315 cm^{-1} are due to the $–CH_2$ scissoring and –OH bending vibrations, respectively. The bands at 1061 cm^{-1} are ascribed to the –CH–O–CH stretching.[10] The most notable speciality for the spectrum of CMC–SPMNCs is the appearance of a strong peak at 593 cm^{-1}, which could be attributed to the Fe–O bond vibration from the CMC-Fe complex. As compared with the characteristic Fe–O absorption bands of bulk Fe_3O_4 (570 and 375 cm^{-1}), that of CMC-modified Fe_3O_4 shifted to a higher wavenumber. The phenomenon suggests that the Fe–O bond absorption arises from Fe–O–C(O)–MC on the surface of the clusters rather than Fe–O–H, because more electronegative –O–C(O)–MC can enhance the bond force constant for Fe–O bond and hence shift the band to a higher wavenumber.[13] These evidences not only confirm the existence of CMC in the clusters, but also indicate that CMC is connected to iron through coordination bonds. Since the absorption characters of CMC remain almost unchanged for CMC–SPMNCs, CMC and iron salt very likely undergo a simple metal displacement reaction. It is noteworthy that plenty of carboxylate groups are not yet coordinated on the surface of the clusters, which enable CMC–SPMNCs to further conjugate with other guest molecules such as antibodies or drugs.

The variable-field magnetization data for CMC–SPMNCs at 300 K were acquired on SQUID. As shown in Fig. 6, the saturation magnetization value is 68.7 emu g^{-1}, which is lower than

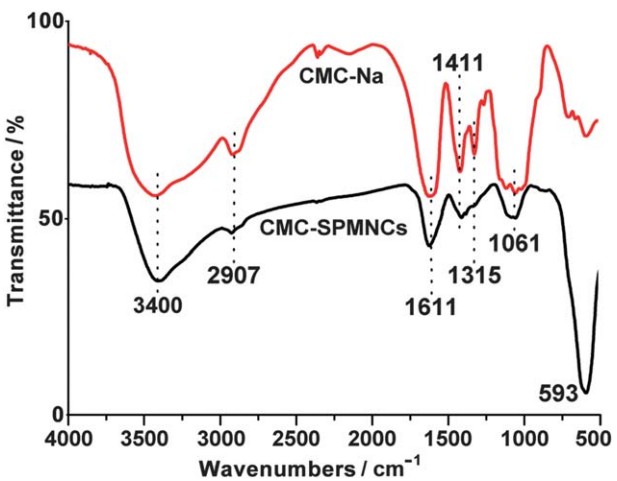

Fig. 5 FT-IR spectra of CMC-Na and CMC–SPMNCs.

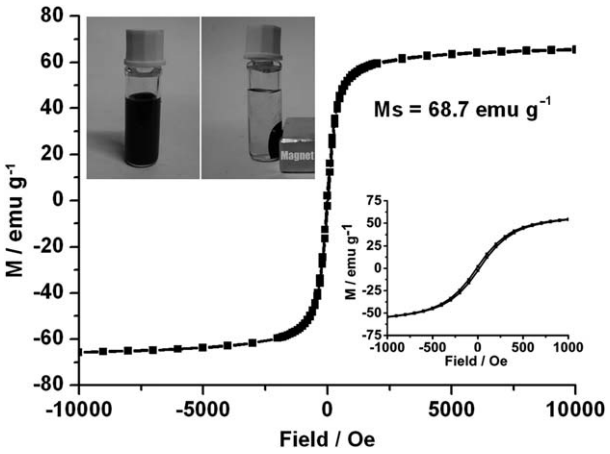

Fig. 6 Variable-field magnetization curves for CMC–SPMNCs at 300 K. Right inset, enlarged curves in the field range of −1000 to 1000 Oe; left inset, status of CMC–SPMNCs in water with or without an external magnet.

that of the bulk Fe_3O_4 (89 emu g^{-1}) but is higher than that of other modified Fe_3O_4 nanoparticles.[6c,14] The difference in saturation magnetization value between CMC–SPMNCs and the bulk Fe_3O_4 may result from the small particle size effect. This phenomenon has been explained in terms of noncollinear spin arrangement at or near the surface of the particles.[15] Additionally, the nonmagnetic CMC component and the possible amorphous impurities on the surface can also reduce the total magnetization. Remanence and coercivity are almost undetectable in the enlarged curves (right inset in Fig. 6), indicating that the clusters possess superparamagnetic properties at room temperature. Owing to the abundant carboxylate groups on the surface of the clusters, CMC–SPMNCs are well dispersed in water (left inset in Fig. 6). The drastic decrease of magnetization after advanced surface modifications and potential aggregation of nanoparticles in capillaries are the major challenges to the development of nanoparticle-based magnetic drug delivery systems. The relatively large magnetization and superb water dispersibility suggest that CMC–SPMNCs can response strongly to the external magnetic field and avoid aggregation in blood capillaries when the magnetic field is removed. These features are essential to magnetic drug carriers for medical application.

Fabrication and characterization of CMDP–CMC–SPMNCs

The active pharmacophore CMDP, a dechlorinated derivative of CDDP, was loaded onto the nanoclusters by two steps. Firstly, CDDP was activated by removing one of the chloride anions to form CMDP;[16] secondly, CMDP was tethered to CMC–SPMNCs through coordination with the carboxylate groups on the surface of the clusters to form the CMDP–CMC–SPMNC conjugate.

The shape and dispersibility of CMDP–CMC–SPMNC were examined by SEM. As shown in Fig. 7, the conjugate particles disperse well as CMC–SPMNCs did. The hydrodynamic diameters of CMDP–CMC–SPMNCs were determined by a dynamic light scattering (DLS) experiment, which gave a mean diameter of 290.6 nm (left inset in Fig. 7), suggesting that the

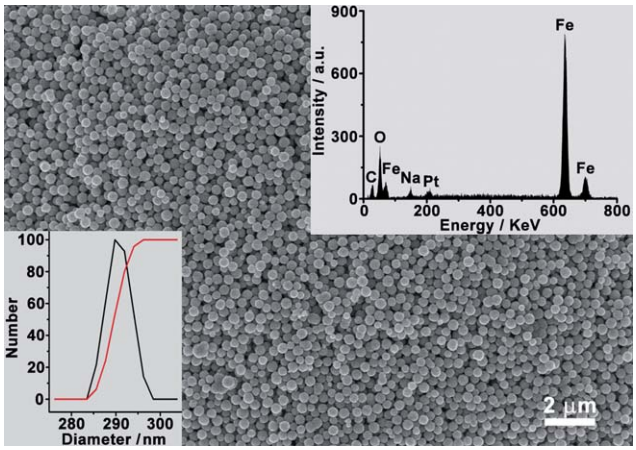

Fig. 7 The SEM image of CMDP–CMC–SPMNCs. Insets are the size distribution of the particles determined by DLS (left) and the EDX spectrum (right), respectively.

conjugate still exists in the form of clusters and disperses separately in aqueous solution. The particle size is just within the dimension range (50–300 nm) of magnetic iron oxide nanoparticles suitable for drug carriers. On such an occasion, particles below 50 nm do not have sufficient magnetic tractive forces to overcome opposing forces from Brownian motion, viscous drag, and sedimentation;[17] while those over 300 nm are unable to extravasate into the interstitial space of the tumor and are rapidly cleared by the liver and spleen,[18] resulting in either poor drug accumulation at the target site or a short circulation half-life. In the EDX spectrum (right inset in Fig. 7), Pt peak is observed in addition to Fe, O, and C peaks from CMC–SPMNCs. The incorporation of platinum in CMDP–CMC–SPMNCs is further demonstrated by XPS measurements (Fig. 8). Besides the photoelectron peaks of Fe2p, O1s, and C1s presented at 700, 530, 285 eV, respectively, Pt4f peaks centered at 73 eV is also observed in the spectrum. In the close up view of the Pt4f region (inset in Fig. 8), two peaks are observed at 72.5 and 75.8 eV for $Pt4f_{7/2}$ and $Pt4f_{5/2}$, respectively, which could be assigned to the binding energy of Pt^{II} in Pt–O–C(O)–MC.[19] XPS confirms the presence of Pt^{II} and formation of the Pt–O bond.

The drug carrying capacity of CMC–SPMNCs in different loading conditions was determined by ICP-MS. The optimal loading of CMDP on CMC–SPMNCs is achieved when the pH is around neutral and the loading time is 100 h. The resulting molar ratio of Pt to Fe is about 1/128.

The zeta potential is an indication of surface charge on a particulate species, which plays an important role in determining the solution stability and cellular binding ability of the particles.[6b] The zeta potentials for CMC–SPMNCs were thus determined before and after the loading of pharmacophore. In comparison with the zeta potential of CMC–SPMNCs (−31 mV), that of CMDP–CMC–SPMNCs decreased to −25 mV. This variation shows that the negatively charged carboxylate groups on CMC–SPMNCs were neutralized by the positively charged CMDP during the conjugation.[20]

The magnetization of CMDP–CMC–SPMNCs was determined as described above. The superparamagnetic properties are well retained in the conjugate, in that the magnetization value is 61.7 emu g^{-1}, merely somewhat lower than that of CMC–SPMNCs (Fig. 9). All these results demonstrate that CMDP can be anchored to CMC–SPMNCs and hence the nanoclusters could serve as magnetic carriers for platinum drugs.

Cytotoxicity and cellular uptake of CMDP–CMC–SPMNCs

The antitumor potential of CMDP–CMC–SPMNCs was tested against HeLa and HepG2 cells by MTT assay with CMC–SPMNCs and CDDP as the controls. As Fig. 10 shows, CMC–SPMNCs barely exhibit cytotoxicity against the tumor cells. In contrast, CDDP and the conjugate demonstrate a remarkable inhibition towards the growth of cell lines. Their half-maximal inhibitory concentrations (IC_{50}) towards HeLa cells are 2.6 and 0.9 μM, respectively; and those towards HepG2 cells are 5.4 and 4.6 μM, respectively. Therefore, the antitumor activity of the platinum moiety is still retained or even enhanced after the conjugation. The inhibitory effect of CMDP–CMC–SPMNCs may stem from the released active platinum species CMDP, and the releasing mechanism might be similar to that proposed for

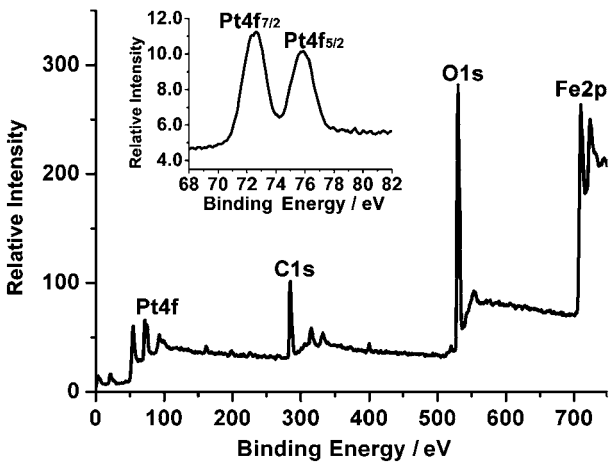

Fig. 8 The XPS spectrum of CMDP–CMC–SPMNCs. Inset shows the high resolution XPS spectrum of Pt4f.

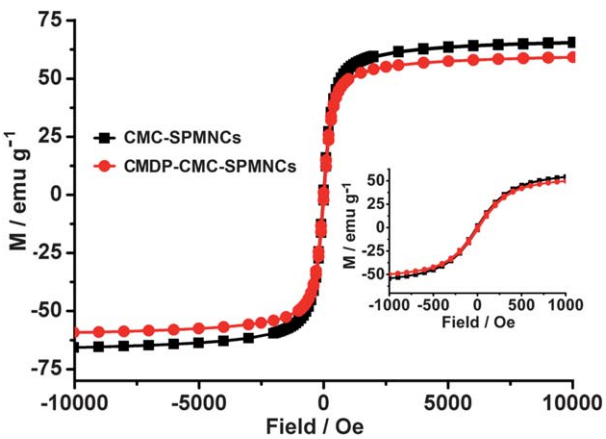

Fig. 9 Magnetization curve of CMDP–CMC–SPMNCs at room temperature, with that of CMC–SPMNCs as the reference. Inset shows the enlarged curves in the field range of −1000 to 1000 Oe.

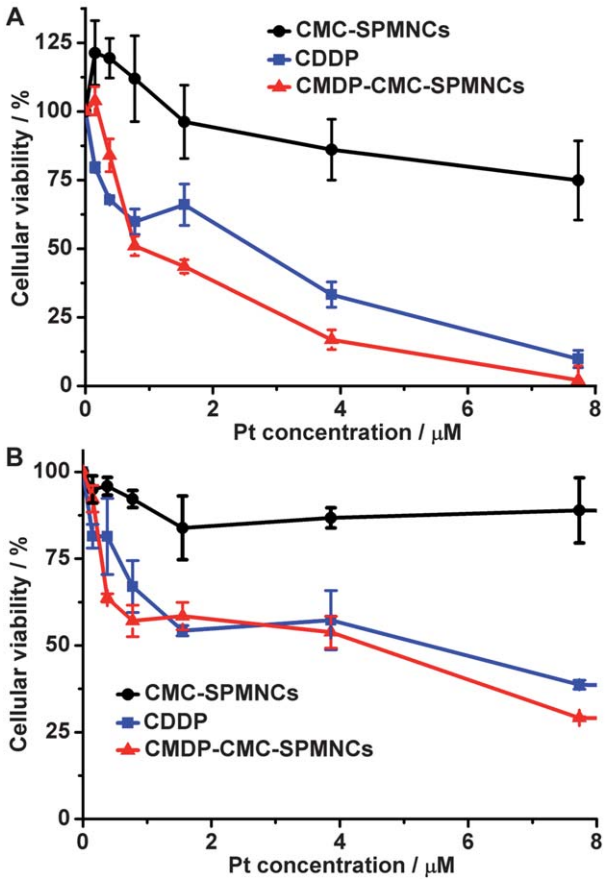

Fig. 10 Cytotoxicity of CMDP–CMC–SPMNCs against the human cervical cancer cell line HeLa (A) and the human hepatocarcinoma cell line HepG2 (B) determined by MTT assay after 72 h, with CMC–SPMNCs and CDDP as the references.

other platinum delivery systems.[3a,4d,6d] In this process, the acidic microenvironment of cancer cells could facilitate the dissociation of platinum pharmacophore from the conjugate.[21]

The time-dependent quantitative cellular uptake of CDDP and CMDP–CMC–SPMNCs by HeLa cells was determined with ICP-MS to discover the pharmacokinetic differences between them. As listed in Table 1, although the platinum uptake of both CDDP and CMDP–CMC–SPMNCs increases with the incubation time, that of the latter is significantly higher (*ca.* 3-fold). The results suggest that the conjugate can more readily be internalized by the tumor cells. A similar phenomenon has been observed in the macromolecule-based delivery system for platinum drugs and the mechanism of internalization was believed to be *via* endocytosis.[22] Since reduced cellular uptake is one of the major

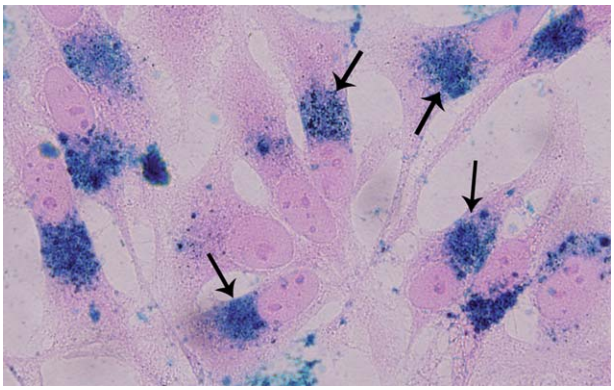

Fig. 11 Photomicrograph for the Prussian blue staining of HepG2 cells incubated at 37 °C for 72 h with CMDP–CMC–SPMNCs (4.6 μM) in culture medium. Arrows point to the aggregating places of iron.

mechanisms for the resistance to platinum drugs,[23] the enhanced platinum uptake of the conjugate is particularly meaningful for defeating the lingering CDDP resistance. Interestingly, the molar ratio of Pt to Fe in the cells is lower than that in original CMDP–CMC–SPMNCs (1/128) and keeps decreasing with the incubation time; this may result from the continuous release of CMDP from the conjugate and subsequent efflux of platinum from the cells.

Finally, iron-specific Prussian blue staining was performed to substantiate the above speculation. Prussian blue staining is one of the most sensitive histochemical tests for detecting the presence of iron in cells. Iron deposits in cells form the Prussian blue dye in place, which can be visualized as blue deposits.[24] As the photomicrograph shows in Fig. 11, blue areas can be clearly observed in the cytoplasm, suggesting that CMDP–CMC–SPMNCs have been internalized by HepG2 cells. However, the iron-containing particles seem to aggregate only at the periphery of the nucleus; therefore, the expected DNA interference is most likely caused by the released CMDP.

Conclusions

Targeted delivery systems are a tempting means for combating the general toxicity of platinum drugs. In this study, superparamagnetic magnetite nanocrystal clusters modified by carboxymethylcellulose have been prepared and the drug loading capacity of the clusters have been tested by different methods. Our intention is to obtain a magnetic drug carrier that can transport platinum drug preferentially to its biological target by making use of a magnetic field. As expected, the drug carrier not only exhibits excellent magnetisability and water dispersibility,

Table 1 Cellular uptake of CDDP and CMDP–CMC–SPMNCs by HeLa cells in terms of platinum or iron content

		Content (ng/10^5 cells) or molar ratio		
Sample	Metal	6 h	12 h	24 h
CDDP	Pt	2.1 ± 0.4	3.9 ± 0.1	4.6 ± 0.2
CMDP–CMC–SPMNCs	Pt	7.4 ± 1.6	11.2 ± 2.6	14.8 ± 2.6
	Fe	594 ± 91	934 ± 80	1363 ± 131
	Pt/Fe	1/279	1/291	1/320

but also significantly improves the cellular uptake of platinum drugs. The cytotoxicity of the drug-carrier conjugate is higher than or at least comparable to that of cisplatin. The advantages of this drug delivery system include the simplicity of preparation, multifunctionality of the particles, and high loading capacity of the carrier. In addition, this approach may be further developed into a promising strategy for targeted delivery of other drugs or biofunctional molecules.

Acknowledgements

We appreciate the financial support from the National Natural Science Foundation of China (Grants 90713001, 21021062, 30870554) and the National Basic Research Program of China (Grant 2011CB935800).

References

1 (*a*) M. Galanski, M. A. Jakupec and B. K. Keppler, *Curr. Med. Chem.*, 2005, **12**, 2075–2094; (*b*) L. Kelland, *Nat. Rev. Cancer*, 2007, **7**, 573–584.
2 (*a*) C. A. Rabik and M. E. Dolan, *Cancer Treat. Rev.*, 2007, **33**, 9–23; (*b*) K. Barabas, R. Milner, D. Lurie and C. Adin, *Vet. Comp. Oncol.*, 2008, **6**, 1–18.
3 (*a*) S. van Zutphen and J. Reedijk, *Coord. Chem. Rev.*, 2005, **249**, 2845–2853; (*b*) X. Y. Wang and Z. J. Guo, *Dalton Trans.*, 2008, 1521–1532.
4 (*a*) Z. Yang, X. Y. Wang, H. J. Diao, J. F. Zhang, H. Y. Li, H. Z. Sun and Z. J. Guo, *Chem. Commun.*, 2007, 3453–3455; (*b*) K. Cheng, S. Peng, C. J. Xu and S. H. Sun, *J. Am. Chem. Soc.*, 2009, **131**, 10637–10644; (*c*) R. M. Xing, X. Y. Wang, C. L. Zhang, Y. M. Zhang, Q. Wang, Z. Yang and Z. J. Guo, *J. Inorg. Biochem.*, 2009, **103**, 1039–1044; (*d*) S. Dhar, W. L. Daniel, D. A. Giljohann, C. A. Mirkin and S. J. Lippard, *J. Am. Chem. Soc.*, 2009, **131**, 14652–14653; (*e*) Z. Q. Xue, M. X. Lin, J. H. Zhu, J. F. Zhang, Y. Z. Li and Z. J. Guo, *Chem. Commun.*, 2010, **46**, 1212–1214.
5 (*a*) C. Sun, J. S. H. Lee and M. Q. Zhang, *Adv. Drug Delivery Rev.*, 2008, **60**, 1252–1265; (*b*) M. Arruebo, R. Fernández-Pacheco, M. R. Ibarra and J. Santamaría, *Nano Today*, 2007, **2**, 22–32.
6 (*a*) T. Neuberger, B. Schöpf, H. Hofmann, M. Hofmann and B. von Rechenberg, *J. Magn. Magn. Mater.*, 2005, **293**, 483–496; (*b*) C. J. Sunderland, M. Steiert, J. E. Talmadge, A. M. Derfus and S. E. Barry, *Drug Dev. Res.*, 2006, **67**, 70–93; (*c*) M. Guo, Y. Yan, H. K. Zhang, H. S. Yan, Y. J. Cao, K. L. Liu, S. R. Wan, J. S. Huang and W. Yue, *J. Mater. Chem.*, 2008, **18**, 5104–5112; (*d*) C. J. Xu, B. D. Wang and S. H. Sun, *J. Am. Chem. Soc.*, 2009, **131**, 4216–4217; (*e*) V. I. Shubayev, T. R. Pisanic II and S. Jin, *Adv. Drug Delivery Rev.*, 2009, **61**, 467–477.
7 (*a*) J. Yang, C.-H. Lee, H.-J. Ko, J.-S. Suh, H.-G. Yoon, K. Lee, Y.-M. Huh and S. Haam, *Angew. Chem., Int. Ed.*, 2007, **46**, 8836–8839; (*b*) D. Y. Chen, M. J. Jiang, N. J. Li, H. W. Gu, Q. F. Xu, J. F. Ge, X. W. Xia and J. M. Lu, *J. Mater. Chem.*, 2010, **20**, 6422–6429; (*c*) R. Hao, R. J. Xing, Z. C. Xu, Y. L. Hou, S. Gao and S. H. Sun, *Adv. Mater.*, 2010, **22**, 2729–2742.
8 (*a*) P. Dames, B. Gleich, A. Flemmer, K. Hajek, N. Seidl, F. Wiekhorst, D. Eberbeck, I. Bittmann, C. Bergemann, T. Weyh, L. Trahms, J. Rosenecker and C. Rudolph, *Nat. Nanotechnol.*, 2007, **2**, 495–499; (*b*) A. Amirfazli, *Nat. Nanotechnol.*, 2007, **2**, 467–468.
9 (*a*) J.-H. Lee, Y.-M. Huh, Y. Jun, J. Seo, J. Jang, H.-T. Song, S. Kim, E.-J. Cho, H.-G. Yoon, J.-S. Suh and J. Cheon, *Nat. Med.*, 2007, **13**, 95–99; (*b*) J.-H. Park, G. von Maltzahn, L. Zhang, M. P. Schwartz, E. Ruoslahti, S. N. Bhatia and M. J. Sailor, *Adv. Mater.*, 2008, **20**, 1630–1635; (*c*) J. Ge, Y. Hu, M. Biasini, W. P. Beyermann and Y. Yin, *Angew. Chem., Int. Ed.*, 2007, **46**, 4342–4345.
10 M. N. Nadagouda and R. S. Varma, *Biomacromolecules*, 2007, **8**, 2762–2767.
11 (*a*) J. Ge, Y. Hu, M. Biasini, C. Dong, J. Guo, W. P. Beyermann and Y. Yin, *Chem.–Eur. J.*, 2007, **13**, 7153–7161; (*b*) S. H. Liu, R. M. Xing, F. Lu, R. K. Rana and J.-J. Zhu, *J. Phys. Chem. C*, 2009, **113**, 21042–21047; (*c*) M. Descostes, F. Mercier, N. Thromat, C. Beaucaire and M. Gautier-Soyer, *Appl. Surf. Sci.*, 2000, **165**, 288–302.
12 C. O'Connell and D. Dollimore, *Instrum. Sci. Technol.*, 1999, **27**, 13–21.
13 (*a*) R. D. Waldron, *Phys. Rev.*, 1955, **99**, 1727–1735; (*b*) M. Ma, Y. Zhang, W. Yu, H.-Y. Shen, H.-Q. Zhang and N. Gu, *Colloids Surf., A*, 2003, **212**, 219–226.
14 Y. Ding, Y. Hu, L. Y. Zhang, Y. Chen and X. Q. Jiang, *Biomacromolecules*, 2006, **7**, 1766–1772.
15 K. V. P. M. Shafi, A. Ulman, A. Dyal, X. Yan, N.-L. Yang, C. Estournès, L. Fournès, A. Wattiaux, H. White and M. Rafailovich, *Chem. Mater.*, 2002, **14**, 1778–1787.
16 J. F. Mao, Y. M. Zhang, J. H. Zhu, C. L. Zhang and Z. J. Guo, *Chem. Commun.*, 2009, 908–910.
17 C. T. Yavuz, J. T. Mayo, W. W. Yu, A. Prakash, J. C. Falkner, S. Yean, L. Cong, H. J. Shipley, A. Kan, M. Tomson, D. Natelson and V. L. Colvin, *Science*, 2006, **314**, 964–967.
18 L. Zhang, F. Yu, A. J. Cole, B. Chertok, A. E. David, J. Wang and V. C. Yang, *AAPS J.*, 2009, **11**, 693–699.
19 (*a*) X. Zhang and K.-Y. Chan, *Chem. Mater.*, 2003, **15**, 451–459; (*b*) T. C. Deivaraj, W. X. Chen and J. Y. Lee, *J. Mater. Chem.*, 2003, **13**, 2555–2560.
20 M. K. Yu, Y. Y. Jeong, J. Park, S. Park, J. W. Kim, J. J. Min, K. Kim and S. Jon, *Angew. Chem., Int. Ed.*, 2008, **47**, 5362–5365.
21 I. F. Tannock and D. Rotin, *Cancer Res.*, 1989, **49**, 4373–4384.
22 J. R. Rice, J. L. Gerberich, D. P. Nowotnik and S. B. Howell, *Clin. Cancer Res.*, 2006, **12**, 2248–2254.
23 D. Wang and S. J. Lippard, *Nat. Rev. Drug Discovery*, 2005, **4**, 307–320.
24 J. A. Frank, B. R. Miller, A. S. Arbab, H. A. Zywicke, E. K. Jordan, B. K. Lewis, L. H. Bryant Jr and J. W. M. Bulte, *Radiology*, 2003, **228**, 480–487.